

Ice Core Drilling and the Related Observations at SE-Dome site, southeastern Greenland Ice Sheet

Yoshinori IIZUKA^{1*}, Sumito MATOBA¹, Masahiro MINOWA^{1,2}, Tetsuhide YAMASAKI³,
Kaoru KAWAKAMI^{1,4}, Ayako KAKUGO¹, Morihiro MIYAHARA⁵, Akihiro HASHIMOTO⁶,
Masashi NIWANO⁶, Tomonori TANIKAWA⁶, Koji FUJITA² and Teruo AOKI⁷

¹ Institute of Low Temperature Science, Hokkaido University, Sapporo 060-0819, Japan

* iizuka@lowtem.hokudai.ac.jp

² Graduate School of Environmental Studies, Nagoya University, Nagoya 464-8601, Japan

³ Avangnaq, Osaka 596-0094, Japan

⁴ Graduate School of Environmental Science, Hokkaido University, Sapporo 060-0810, Japan

⁵ Anori Corporation, Kobe 662-0957, Japan

⁶ Meteorological Research Institute, Tsukuba, 305-0052, Japan

⁷ National Institute of Polar Research, 10-3, Tachikawa, Tokyo 190-8518, Japan

(Received July 19, 2021; Revised manuscript accepted August 26, 2021)

Abstract

In order to construct reliable deposited-aerosol database on the Anthropocene (from 1850 to 2020), we obtained a 250-meter-long ice core from the Southeastern Greenland Dome on May and June 2021, where is one of the highest accumulation domes in Greenland. The age of the ice core at a depth of 250 m was roughly estimated to be AD 1827 based on the timescale from a previously analyzed shallower ice core. The age of the sampled ice core satisfied the prerequisite conditions for constructing aerosol deposition database for Anthropocene. In addition, surface elevation, borehole temperatures, and internal stratigraphy of the ice sheet were performed, and meteorological and snow-pit observations were also conducted. Furthermore, we sampled aerosol and snow from the ice sheet for chemical and physical analyses.

Key words: Greenland Ice Sheet, Ice core, High accumulation, SE-Dome, Anthropocene

1. Introduction

Polar ice sheets are good archives of paleo-environmental events. In particular, the ice sheets domes are better locations for precise reconstruction of paleo-environmental events. Therefore, several ice cores have been drilled and analyzed from ice sheet domes (Watanabe *et al.*, 2003, EPICA community members, 2006). The previously studied cores from ice sheets are mostly in areas with a low accumulation rate as they are located in inland dry areas. Such cores allow the reconstruction of past environments up to several hundred thousand years old with high quality measurements. However, ice cores in areas with low accumulation rates have the limitation of low temporal resolution, which hinders the environmental reconstruction of the recent epochs such as the Anthropocene (from 1850 to present) with seasonal resolution. Also, since Antarctica does not likely deposit anthropogenic aerosol, ice cores from Greenland with high accumulation rates are suited to environmental reconstruction of the Anthropocene.

We have focused on the reconstruction of recent

environmental changes since 2014 by analyzing dome cores on ice sheets with high accumulation rate. We selected southeastern Greenland dome (SE-Dome), which is one of the highest accumulation domes in Greenland (Iizuka *et al.*, 2016; 2017). Our previous study of the SE-Dome ice core has indicated that the high accumulation rate of the SE-Dome allows ice core dating at a high temporal resolution with an error of less than two months (Furukawa *et al.*, 2017). This error range enables us to construct seasonal flux of aerosol proxies preserved in the ice core. Furthermore, due to the high accumulation rate of SE-Dome, any post depositional effects on the aerosol species are negligible (Iizuka *et al.*, 2018). The SE-Dome ice core even preserves nitrate aerosol without significant post depositional effect, which is lost from ~20% of the deposited fluxes in other domes of Greenland (Zatko *et al.*, 2016). Thus, the ice core from SE-Dome represents one of the best ice cores to reconstruct recent aerosol fluxes with seasonal resolution. Earlier studies have reported that the oxygen isotopic composition of sulfate in the SE-Dome ice core exhibit an increasing trend since the 1960s, implying an enhanced role of acid-dependent in-cloud oxidation by ozone in the production

of sulfates since the 1960s (Hattori *et al.*, 2021). In addition, Amino *et al.*, (2021) reported that the annual dust fluxes have enhanced after 2000, primarily due to increasing dust flux during autumn. The observation suggests an increase in dust emissions after 2000 due to increase in snow-free land on the east coast of Greenland owing to global warming (Amino *et al.*, 2021).

However, the previously studied ice core was 90.45 m in length, and contained environmental proxies of only the recent 60 years. The short-term reconstruction is a limitation of high accumulation ice core. In general, Greenlandic ice cores with ~ 100 m length enable the proper reconstruction of events that occurred in the past 200 to 300 years (Iizuka *et al.*, 2017). However, the general ice cores are difficult to precise annual counting of seasonal proxies such as $\delta^{18}\text{O}$ due to the proxies disturbing by low accumulation rate (Furukawa *et al.*, 2017). Thus, the previously studied ice core did not contain the entire seasonal aerosol fluxes from the Anthropocene (1850–present). To overcome this limitation, we conducted an expedition and drilled longer ice cores from the SE-Dome region. In this paper, we report the logistics and the ice core drilling procedures along with

the glaciological and meteorological observations.

2. Research Area

The new drilling site ($67^{\circ}11'30.14328''\text{N}$, $36^{\circ}28'12.77075''\text{W}$, 3160.7 m a.s.l.), referred as SE-Dome, is located at 185 km north of the town Tasiilaq in southeastern Greenland (Fig. 1). The main Greenland ice divide has a fork at the southern Summit (GRIP/GISP2). In the southern area of the fork, the two ice divides: one extends southwest towards Narsarsuaq through Dye 3 while the other extends southeast towards Tasiilaq. Due to the presence of a high mountain under the ice sheet (Bamber *et al.*, 2013) and high snow accumulation (Burgess *et al.*, 2010), the elevation of SE-Dome is beyond 3,000 m above sea level (Fig. 1). The new drilling site was situated at 5 km west from the previous drilling site. The real summit of the SE-Dome area might be located along the line between the previous and new drilling site. However, the difference between the elevations of the real summit and new the drilling site was less than 20 m (less than 1% of the elevation change) (Fig. 1), therefore, ice cores obtained from the new drilling site was con-

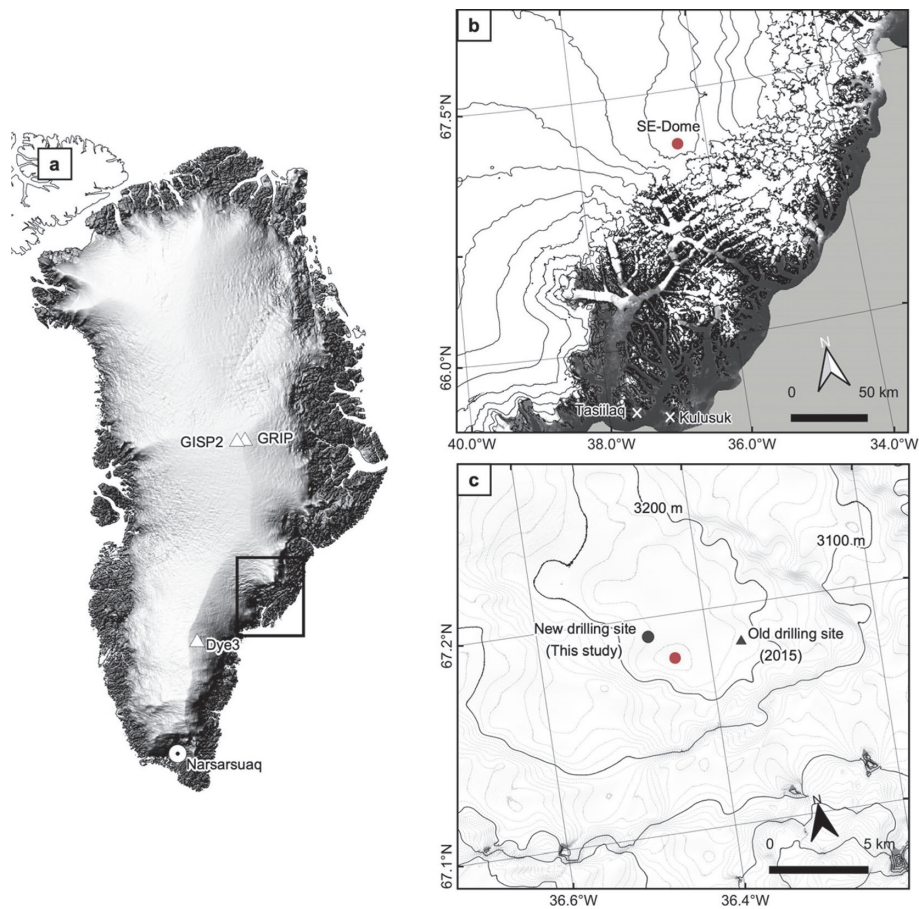


Fig. 1. (a) Map of Greenland Ice Sheet. The white triangles indicate the previous ice core drilling sites surrounding the SE-Dome. (b) Satellite mosaic image and topography map showing the location of SE-Dome in the southeast Greenland. The images were acquired by MODIS instrument. Surface topography is constructed based on GIMP DEM with contour intervals of 250 m. (c) Enlarged topography map of the SE-Dome with contour intervals at every 10 m. The red circle indicates the highest point of the dome estimated based on the ArcticDEM data. The grey circle and the triangle indicate the drilling points of this study ($67^{\circ}11'30.14328''\text{N}$, $36^{\circ}28'12.77075''\text{W}$) and the previous study, respectively.

sidered to be a typical dome ice core.

Several modelling and satellite analyses have provided information on the characteristics of the Greenland Ice Sheet, including the SE-Dome area (Burgess *et al.*, 2010; Fettweis *et al.*, 2020). The following features characterize the SE Dome areas: 1) it is one of the highlands in Greenland with an elevation of more than 3,000 m above sea level; 2) the region has relatively cold air with annual average temperature lower than -20°C ; 3) it is one of the domes in Greenland with the highest rate of accumulation. Although the results from previous ice core (about 1 m w.e. yr^{-1}) support the above model and satellite analyses (Iizuka *et al.*, 2016; 2017; Furukawa *et al.*, 2017), Fettweis *et al.* (2020) suggested that more data related to in situ surface mass balance are required in the southeast accumulation zone, where the spread can reach 2 m w.e. yr^{-1} due to large discrepancies in modelled snowfall accumulation. An ice core obtained from the SE-Dome has an advantage of being the representative of the highest accumulation dome in Greenland and for preserving high quality proxy due to the prevailing cold temperature. These advantages enabled us to reconstruct the anthropogenic aerosol deposition from North America and Europe beneath the Icelandic low with high temporal resolution.

3. Participants

The project participants included:

SE-Dome site (5 members)

Sumito Matoba (Hokkaido University), Leader and chief driller.

Tetsuhide Yamasaki (Avangnaq), Logistics and risk management, and weather observation.

Masahiro Minowa (Hokkaido University), Driller, GPS/GPR measurements, and borehole measurement.

Kaoru Kawakami (Hokkaido University), Responsible for ice-core processing, snow pit observation, and aerosol sampling.

Yoshinori Iizuka (Hokkaido University), Chief of Logistics, driller, and snow pit observation.

Supporting members in Japan (7 members)

Teruo Aoki (National Institute of Polar Research), Leader of domestic response headquarters and weather forecast.

Ayako Kakugo (Hokkaido University), Responsible for logistics and domestic response headquarters.

Morihiro Miyahara (Anori Corporation), Responsible for drilling mechanics and drilling support.

Koji Fujita (Nagoya University), Responsible for logistics, domestic response headquarters, and weather analyses.

Akihiro Hashimoto, Masashi Niwano, and Tomonori Tanikawa (Meteorological Research Institute), Responsible for weather forecast.

4. Itinerary

Our team chartered a de Havilland Canada DHC-6 Twin Otter from Norlandair in Akureyri, Iceland, and flew from Kulusuk to the observation site. The total weight of the equipment carried along was $\sim 3,600\text{ kg}$, where the volume of gasoline for the generator was 300 L and the volume of kerosene for cooking was 140 L. On 9th and 10th May 2021, five personnel including the drill system, fuel, food, and sleeping tents were flown to the observation site. We set up the drill system on 11th May and drilled ice core from 12th May to 2nd June. All scheduled field studies were completed by 12th June 2021.

On 13th and 14th June, all personnel, equipment, the ice core, and snow samples were flown from the observation site to Kulusuk. The ice cores were temporarily stored in a freezer below -18°C at the Kulusuk airport. The ice cores will be transported by a 40 ft reefer from Kulusuk via Aalborg to the Institute of Low Temperature Science at Hokkaido University in mid-October. During transit by Blue Water Shipping A/S (Denmark) and Maruzen Syowa Japan Co., Ltd., the ice cores were kept below -25°C .

It is worthy to describe that this project was conducted during Covid-19 disaster that surfaced across the world from February 2019. Therefore, we had to postpone this project from spring 2020 to spring 2021. We had to seek permission for this field study to Greenland (Denmark was one of the Level 3 (Avoid all travel) countries issued by the Ministry of Foreign Affairs of Japan). We also had to take permission for conducting field work on remote areas of Greenland and acquire a residence permit from Greenlandic government. We stayed 5 days in Nuuk and 14 days in Tokyo for quarantine, and had to undertake several tests for the coronavirus. As a result, the term and budget of the project increased approximately twice than the planned. We responded by combining our budgets of FY2020 and FY2021 Kakenhi.

5. Field activities

5.1 Ice-core drilling and borehole temperature measurement

The ice core drill system was an electro-mechanical shallow-type drill manufactured by the Geo Tech Ltd. (Nagoya, Japan) for an expedition in Mount Wrangell, Alaska in 2004 (Kanamori *et al.*, 2008). The winch system and the controller of the drilling system were later developed by Kyushu Olympia Kogyo Co. Ltd. (Miyazaki, Japan) in 2019 specifically for drilling in the studied region. The specifications of the drill system are provided in Table 1. One of the noteworthy characteristics of the drill system is its 2528 mm long core barrel, which enables to obtain 1 m long ice core. Another characteristic is a 750 watt three-phase inverter motor used in the winch motor. The motor enables the drill to ascend and descend with high speed. We used a generator (YAMAHA model

Table 1. Specifications of the drill system.

Table Specification of the drill system

Drill	
Core length	1000mm
Drill jacket length/diameter	2580mm / 125mm
Drill barrel length/diameter	2528mm / 101.6mm
Material of barrel	Pure titanium
Drill motor	Permanent magnet direct current motor, 200V/500W 4,000rpm
Reduction drive	Harmonic drive system; reduction ratio 1/80
Anti-torque type	Leaf spring type; stainless spring steel
Cutter mount	Outer 125mm, inner 97.8mm, No. of cutter 3, No. of catcher 3
Winch system and mast	
Winch drum	Cast aluminum (AC4C), inner 280mm, outer 394mm, width 190mm
Winch motor	Three-phase inverter motor, 4 plugs, 750W
Reduction drive	Harmonic drive system; reduction ratio 1/50
Cable	4 core-wire armored cable, ϕ 4.72 mm
Mast type	Tilting type
Mast length	2913mm above surface, 301mm under surface
Materials of base and mast	Aluminum

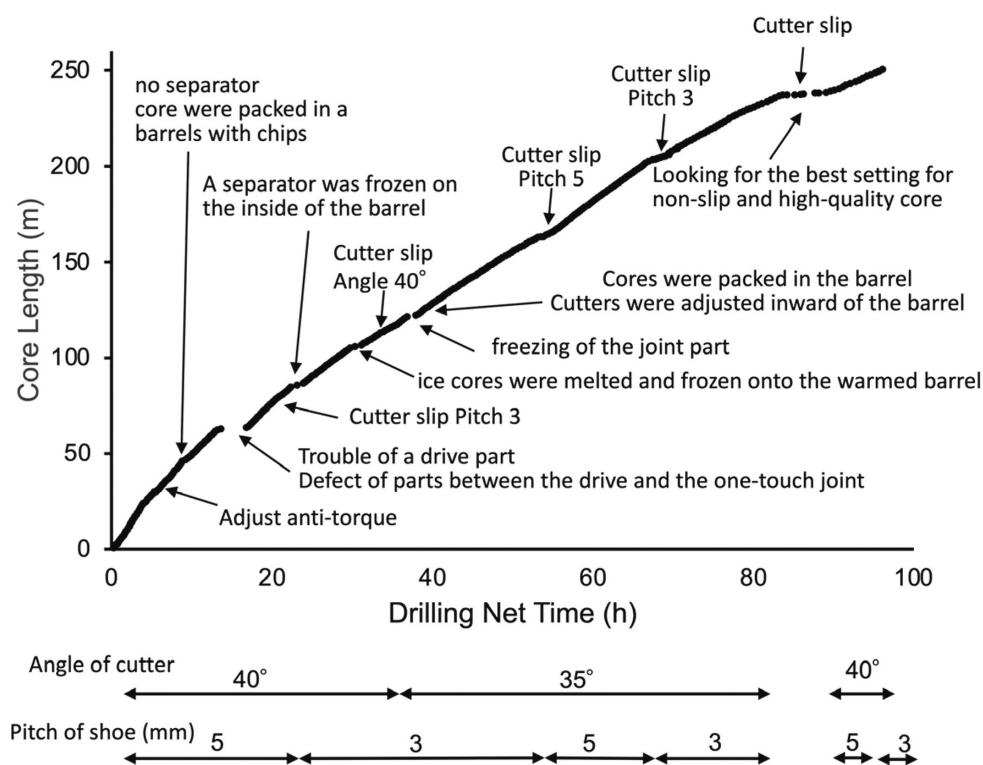


Fig. 2. Relationship between drilling net time (h) and core length (m) based on observations.

EF2500i) with a four-cycle, single-cylinder gasoline engine for the drilling operations. For usage at high-elevations, we replaced the fuel spray nozzle in the carburetor with one with a smaller hole.

The drilling operations are summarized in Figure 2. We set up the drilling tent on 10th May and built the drilling system in the tent on 11th May (Fig. 3a). The

winch base was fastened onto timbers with bolts, and the winch base and timbers were attached to the snow-covered surface with snow and water. We began ice core drilling from 1.27 m below the surface on 12th May at 8:40; however, on 24th May at 16:10, we had to suspend drilling at the depth of 234.5 m because of a strong blizzard and the subsequent collapse of the drilling tent

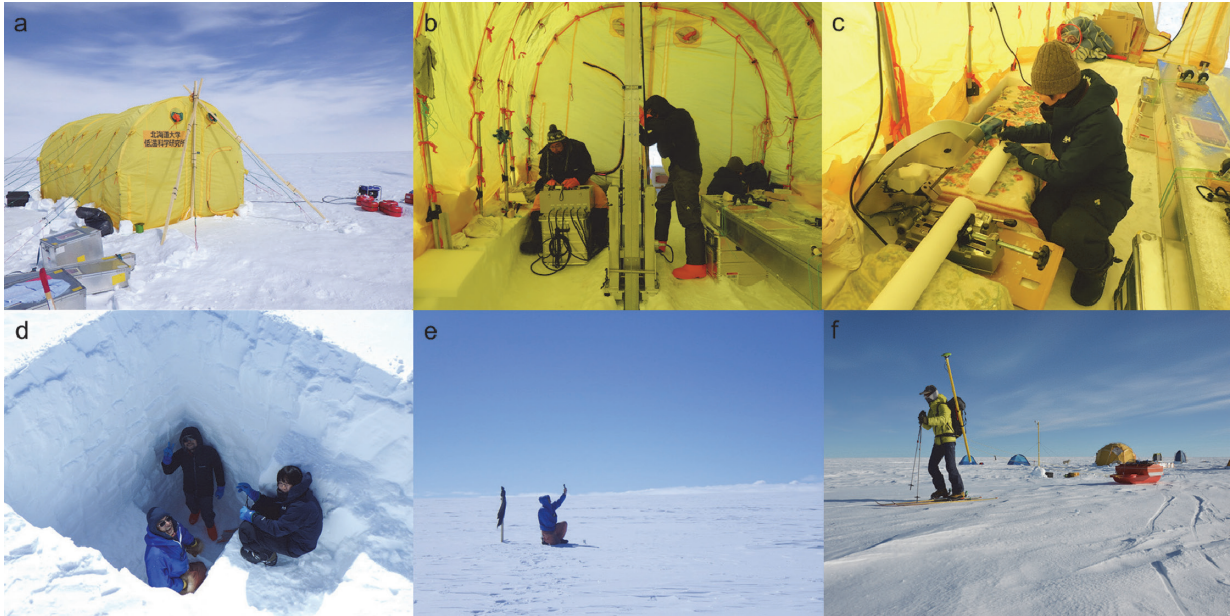


Fig. 3. Pictures of the SE-Dome observation site. a) Drilling tent; b) drilling operation; c) ice core processing; d) pit observation; e) Meteorological observation; and f) GPS and GPR measurements.

(Fig. 3b). After repairing the drilling tent, we re-started drilling on 27th May. However, we re-stopped drilling on 28th May at 10:42 at a depth of 250.5 m because of another strong blizzard. After the blizzard, we attempted to re-start drilling on 2nd June. While drilling the bore hole, the drill was obstructed at the depth of 230 m, and it could not descend further. We rotated the drill cutters while it was obstructed, however, the drill rotated without any resistance and did not cut anything. We attempted to perform similar operations several times, but it was futile. To investigate the condition of the bore hole, we inserted only the drive part of the drill with an anti-torque. The length of the drive part was ~ 0.60 m. The drive part could reach the bottom of the bore hole smoothly. Based on the above observation, we assumed that the bore hole had bent at the depth of 230 m during the drilling process, and the bent bore hole had shrunk during the period when drilling was suspended (29th May to 2nd June). Therefore, the 3.3 m long drill was caught at the shrunk bore hole at 230 m. Since we could not improve the situation, we had to stop the drilling process. We conducted stratigraphic observations of the ice core, and recorded the stratigraphic features and lengths of the ice core over the entire depth of the core (Fig. 3c). The ice core contained fifteen ice layers, whose thicknesses were less than 0.02 m. In the field, ice cores were stored in insulating boxes and transported to the freezer in Kulusuk by a twin otter on 13th and 14th June.

We measured the ice temperature of the borehole wall on 2nd June after the completion of the ice-core drilling. A thermocouple (Ondotori, TR-52i; accuracy $\pm 0.3^\circ\text{C}$) was lowered into the borehole, which measured ice temperature at every 10 m depth for 5 min until it reached 100 m deep into the borehole. On 3rd June, a

300 m long thermistor chain with 40 thermistors (Sanyo Denko, SAN-Thermo) was lowered into the borehole with packs filled with granulated snow. The temperatures obtained by the thermistors were compared with that obtained by a platinum resistance thermometer at ice temperature (0°C). The mean difference between the thermistors was $\pm 0.2^\circ\text{C}$ at 0°C . Each thermistor was placed at intervals of 7.5 m on the cable. We placed 34 thermistors into the borehole, and the lowest thermistor was located at 248.9 m. The rest of the 6 thermistors were attached on a 5.5 m long mast at every 0.5 m from the snow surface to monitor the height and temperature of snow. During daytime, the borehole temperature was measured at every 1 s between 3rd and 6th June. On 7th June, we set the sampling interval to every 1 min for long-term monitoring of borehole temperature. The temperature sampling data with every 1 min will be collected in next spring in 2022.

5.2 Aerosol, precipitation, and surface snow sampling

Aerosol, precipitation, surface snow sampling, and snow pit observation were performed at 150 m windward (northeastward) direction from the drilling site. Aerosols were sampled using filtration method. A single filter pack was fixed at a height of 1.5 m of a 2 m stake. The air going through the filter pack was aspirated at a rate of 2.0L min^{-1} by a diaphragm pump (SIBATA MP- Σ 500 N). A Teflon filter with a pore size of $0.40\ \mu\text{m}$ (Advantec, H040A047 A) was used. We collected aerosols during the following six periods: i) 18:00 on 30th May to 7:00 on 31st May; ii) 19:00 on 1st June to 7:00 on 2nd June; iii) 14:40 on 6th June to 9:00 on 7th June; and iv) 8:45 to 16:00 on 9th June; v) 16:30 on 9th June to 9:50 on 10th June; vi) 18:30 on 11th June to 5:30 on 12th June. After sampling, the

Table 2. Meteorological data recorded at SE-Dome during the field study. Hyphens indicate the absence of measured data.

date	time	weather	wind direction	average (and maximum) wind speeds (m s ⁻¹)	air temperature (°C)	snow temperature (°C)	atmospheric pressure (hpa)	visibility (km)	cloud amount	cloud type
10-May	AM6:25	sunny	NE	1.7(2.8)	-18.7	—	683	>15	2	Cs
11-May	AM5:00	foggy (sunny in upper air)	N	1.8(2.6)	-19.8	-28.1	678	10	0	—
11-May	PM7:35	sunny	S	1.9(2.3)	-17.4	-18.3	680	>15	2	1Cs, 1As
12-May	AM5:00	sunny	SE	2.2(2.5)	-23.4	-26.9	681	15~20	7	4Cs, 3As
12-May	PM7:10	sunny	NE	1.7(2.1)	-19.6	-18.5	680	>15	0+	St
13-May	AM5:00	sunny	NE	2.1(2.6)	-27.3	-29.1	684	>15	0	—
13-May	PM5:00	sunny	NE	1.0(1.2)	-15.9	-17.4	682	>15	0	—
14-May	AM5:00	sunny	NE	2.3(2.8)	-25.9	-30.5	685	>15	0	—
14-May	PM2:05	sunny	NE	1.9(2.3)	-11.9	-16.7	687	>15	0	—
14-May	PM6:00	sunny	NE	1.2(1.4)	-17.4	-18.1	685	>15	0+	Ci
15-May	AM5:00	sunny	SW	0.3(0.5)	-14.1	-30.2	687	>15	0+	Cs
15-May	AM11:10	sunny	E	0.5(0.8)	-7.6	-17.7	687	>15	1	Cs
15-May	PM5:00	sunny	W	0.9(1.2)	-10.4	-14.5	686	>15	1	Cs
16-May	AM5:00	sunny	NE	1.4(1.6)	-15.5	-28.8	686	>15	1	St
16-May	AM11:15	sunny	NE	2.0(2.2)	-11.7	-17.4	686	>15	0	—
16-May	PM4:55	sunny	NE	3.0(3.7)	-14.0	-15.0	685	>15	0	—
16-May	PM10:30	sunny	NE	2.6(3.2)	-24.0	-25.9	683	>15	0	—
17-May	AM5:00	sunny	E	0.8(0.9)	-17.1	-28.5	686	>15	0	—
17-May	AM11:25	sunny	NE	1.1(1.3)	-8.1	-15.2	684	>15	0	—
17-May	PM5:10	sunny	NE	1.5(1.7)	-11.6	-14.2	684	>15	0	—
18-May	AM5:00	sunny	E	2.1(2.6)	-22.0	-29.8	686	>15	0	—
18-May	AM11:00	sunny	NE	3.9(5.1)	-14.2	-16.3	683	>15	0	—
18-May	PM5:00	sunny	NE	3.1(3.7)	-14.8	-15.7	685	>15	0+	St
19-May	AM4:20	sunny	E	2.5(2.9)	-23.2	-28.7	690	>15	0+	Cs
19-May	AM11:40	sunny	S	0.6(0.8)	-8.7	-16.2	688	>15	1-	St
19-May	PM4:35	sunny	NE	2.0(2.4)	-13.2	-13.9	684	>15	1	Cs
20-May	AM1:30	sunny	NE	1.6(1.9)	-21.9	-30.0	686	>15	2	1Cs, 1As
20-May	AM4:55	lightly cloudy	E	1.1(1.3)	-19.0	-30.5	683	>15	8	Cs
20-May	AM11:05	sunny	E	1.9(2.2)	-13.2	-18.6	683	>15	1	Ci
20-May	PM4:55	sunny	SE	0.6(1.0)	-12.8	-15.1	680	>15	1	0+St, 1-Ci
21-May	AM4:55	sunny	E	3.4(4.4)	-23.5	-28.7	681	15	2	1Ci, 1St
21-May	AM11:05	lightly cloudy	E	7.7(10.0)	-16.9	-19.6	676	5~10	9	5Ci, 4St
21-May	PM4:55	blowing snow(sunny in upper air)	E	7.3(9.4)	-19.0	-18.0	674	0.2~0.3	Unobservable	Unobservable
22-May	AM4:45	blowing snow	NE	7.1(10.5)	-21.8	-22.7	672	0.1	Unobservable	Unobservable
22-May	AM10:45	blowing snow(sunny in upper air)	NE	6.9(8.6)	-17.2	-17.6	673	0.1~0.2	Unobservable	Unobservable
22-May	PM4:45	blowing snow(sunny in upper air)	NE	8.1(10.5)	-17.2	-16.4	672	0.1~0.2	2~3	Ci?
23-May	AM5:00	cloudy with drifting snow	NE	4.6(6.3)	-18.2	-18.7	674	0.5	10-	As
23-May	AM11:05	blowing snow(sunny in upper air)	E	7.1(13.4)	-17.9	-17.7	674	0.1	Unobservable	Unobservable
23-May	PM4:50	blowing snow(sunny in upper air)	NE	6.4(7.3)	-17.4	-15.6	674	0.2~0.3	Unobservable	Unobservable
24-May	AM4:45	foggy	NE	4.1(5.0)	-22.5	-23.7	681	0.5~1.0	10	St
24-May	AM11:00	blowing snow(sunny in upper air)	NE	8.3(10.2)	-17.2	-17.1	678	0.1	Unobservable	Unobservable
24-May	AM11:25	—	NE	10.9(13.6)	—	—	—	—	—	—
24-May	PM12:15	—	NE	11.3(13.4)	—	—	—	—	—	—
24-May	PM1:35	—	NE	12.0(14.1)	—	—	—	—	—	—
24-May	PM2:35	—	E	12.2(15.7)	—	—	—	—	—	—
24-May	PM3:30	—	E	11.2(15.6)	—	—	—	—	—	—
24-May	PM4:30	blizzard	E	11.9(13.7)	-17.1	-16.9	676	0	Unobservable	Unobservable
25-May	AM10:30	blizzard	E	13.5(17.1)	-19.1	—	678	0	Unobservable	Unobservable
25-May	PM6:00	blizzard	E	11.6(15.3)	-15.5	-17.2	680	5~10	Unobservable	Unobservable
26-May	AM4:20	snowstorm	E	7.9(9.3)	-15.0	-15.8	687	0.2~0.3	10?	Ns? or As?
26-May	AM11:10	snowstorm	E	8.6(10.2)	-10.2	-15.3	687	0.1~0.2	10?	Ns? or As?
26-May	PM6:15	blowing snow(sunny in upper air)	E	11.4(14.3)	-10.5	-11.3	686	0.5	3	Cu
27-May	AM4:15	blowing snow	E	10.3(12.7)	-10.4	-15.1	689	0.2~0.3	Unobservable	Unobservable
27-May	AM10:45	sunny with drifting snow	NE	5.6(6.9)	-6.2	-9.3	688	5	2	2-St, 0+Ci
27-May	PM4:45	sunny with drifting snow	NE	6.7(7.7)	-6.7	-8.1	686	10~15	2	1St, 1Ci
28-May	AM4:35	sunny with drifting snow	NE	7.5(8.9)	-13.4	-18.5	685	>15	2	St
28-May	AM7:45	snowstorm	NE	10.2(12.8)	-11.1	-14.2	678	0	Unobservable	Unobservable
28-May	AM10:00	blizzard	E	12.8(15.9)	—	—	678	0	—	—

Table 2. (continued)

date	time	weather	wind direction	average (and maximum) wind speeds (m s ⁻¹)	air temperature (°C)	snow temperature (°C)	atmospheric pressure (hpa)	visibility (km)	cloud amount	cloud type
28-May	AM11:00	blizzard	E	10.4(20.7)	—	—	679	0	—	—
28-May	PM3:00	blizzard	E	13.1(16.9)	-8.9	-10.5	679	0	—	—
29-May	AM10:45	snowstorm	E	9.6(12.6)	-9.9	-10.6	672	0.0~0.1	10?	Ns? or As?
29-May	PM6:00	snowstorm	E	9.2(11.2)	-10.3	-10.2	673	0.1	10?	Ns? or As?
30-May	AM4:00	snowstorm	E	10.8(13.4)	-13.5	-14.9	670	0	Unobservable	Unobservable
30-May	AM7:20	blizzard	NE	14.8(17.6)	-12.6	-13.1	663	0	Unobservable	Unobservable
30-May	PM4:40	snowy	E	3.7(4.6)	-11.8	-11.8	667	5	10	As
31-May	AM4:25	sunny	NE	2.8(3.6)	-21.0	-25.0	669	>15	1	St
31-May	PM12:25	sunny	SE	2.6(3.2)	-10.5	-14.1	668	>15	1	1-St, 0+Ci
31-May	PM5:00	sunny	SE	0.8(1.0)	-7.9	-12.3	668	>15	0+	St
1-Jun	AM4:35	sunny	NE	2.5(2.9)	-25.0	-26.7	669	10	3	3St, 0+Ci
1-Jun	PM12:55	blowing snow(sunny in upper air)	NE	5.2(7.7)	-11.3	-12.2	669	2.0~3.0	Unobservable	Unobservable
1-Jun	PM5:20	snowy	NE	3.7(4.9)	-13.1	-13.6	669	5	6	5St, 1Ci
2-Jun	AM4:30	sunny	NE	1.8(2.3)	-24.0	-28.2	670	>15	1-	St
2-Jun	AM10:50	sunny	W	2.6(2.9)	-12.3	-17.6	673	>15	0+	St
2-Jun	PM6:05	sunny	W	1.1(1.3)	-12.5	-15.9	675	10~15	1	1-St, 0+Cu
3-Jun	AM4:00	sunny	NE	0.8(1.0)	-19.2	-27.9	676	>15	0+	St
3-Jun	AM10:30	sunny	NE	0.6(0.8)	-8.0	-19.1	681	>15	1	St
3-Jun	PM6:10	sunny with drifting snow	NE	5.2(6.0)	-13.5	-14.9	679	>15	1	1-St, 0+Ci
4-Jun	AM4:10	cloudy with blowing snow	NE	8.9(10.7)	-16.5	-18.1	678	10	10	As
4-Jun	AM10:25	snowstorm	NE	10.5(12.0)	-12.8	-14.7	681	0.1	Unobservable	Unobservable
4-Jun	PM6:25	snowstorm	NE	6.7(8.1)	-11.4	-12.1	682	0.1	10?	Ns? or As?
5-Jun	AM4:10	snowstorm	NE	8.2(10.0)	-11.0	-11.6	683	0.1	10?	Ns? or As?
5-Jun	AM10:00	snowstorm	NE	7.6(10.9)	-7.7	-10.6	683	0.1	Unobservable	Unobservable
5-Jun	PM6:30	snowstorm	NE	5.5(7.1)	-10.1	-10.2	682	0.2~0.3	10	Ns
6-Jun	AM4:00	cloudy with blowing snow	NE	5.0(6.7)	-9.8	-11.8	685	0.5	10	Ns? or As?
6-Jun	AM10:30	snowy	E	5.1(6.7)	-5.8	-9.3	682	1~5	9	St
6-Jun	PM6:10	snowy	NE	4.9(5.7)	-6.7	-7.4	683	1~2	8	7St, 1Ci
7-Jun	AM3:20	snowy	NE	4.4(5.3)	-10.8	-11.1	681	0.5	10	As
7-Jun	AM11:00	sunny	NE	2.6(3.2)	-6.5	-9.2	683	>15	3	1Cu, 1Ci, 1St
7-Jun	PM6:00	snowy	NE	4.7(5.5)	-9.1	-8.7	677	5~10	10	As or St
8-Jun	AM3:55	sunny	NE	2.1(2.3)	-17.0	-16.9	679	>15	1-	Cs
8-Jun	AM10:55	sunny	NE	3.1(3.6)	-7.3	-12.3	676	>15	1	Cs
8-Jun	PM6:00	sunny	NE	3.6(4.5)	-10.2	-9.1	676	>15	5	0+Cu, 2St, 3Ci
9-Jun	AM3:40	snowy	NE	4.1(4.8)	-13.3	-13.8	676	0.2~0.3	10	As
9-Jun	PM12:30	snowy	NE	4.3(5.2)	-7.7	-8.5	677	1~2	10-	As
9-Jun	PM6:30	snowy	NE	4.8(5.6)	-10.1	-9.5	673	0.1~0.2	10	As
10-Jun	AM3:20	snowstorm	NE	6.3(8.7)	-12.4	-12.0	670	0.1~0.2	10	Ns? or As?
10-Jun	AM10:55	snowy	NE	5.7(7.0)	-7.9	-10.0	669	0.5	10	St
10-Jun	PM6:35	sunny	NE	3.7(4.7)	-11.7	-10.0	669	10~15	7	2Cu, 5Ci
11-Jun	AM3:45	foggy (sunny in upper air)	NE	5.3(6.1)	-17.2	-16.1	671	0.1	Unobservable	Unobservable
11-Jun	AM11:55	lightly snowy	SE	1.6(2.1)	-7.5	-11.2	675	10~15	9+	5Cs, 4+As
11-Jun	PM6:25	snowy	W	2.7(3.3)	-11.9	-10.4	676	5~10	10	As
12-Jun	AM3:30	sunny with snow	SE	2.7(3.1)	-18.0	-15.0	677	10~15	7	3Ns, 4Ac
12-Jun	AM11:05	snowy	W	1.0(1.2)	-5.4	-10.3	677	0.5~1.0	10	As
12-Jun	PM6:00	snowy	NE	3.9(4.9)	-11.8	-9.1	675	1~5	10	As
13-Jun	AM3:20	cloudy	NE	5.6(6.5)	-18.6	-14.2	675	10	10	As
13-Jun	AM5:50	sunny	NE	4.1(5.4)	-19.1	-15.5	674	10~15	5	4Ac, 1St
13-Jun	AM6:50	sunny	NE	3.8(4.7)	-17.7	-14.1	674	>15	1	Cu
13-Jun	AM7:55	sunny	NE	4.3(5.4)	-17.5	-13.6	674	>15	1-	As
13-Jun	AM8:55	sunny with drifting snow	NE	4.6(5.5)	-16.0	-13.4	674	>15	1-	1-Cs, 0+Cu
13-Jun	AM9:55	sunny	E	6.0(6.8)	-15.8	-13.4	674	>15	0+	0+Ac, 0+Cu
13-Jun	PM2:55	sunny	NE	4.3(5.6)	-15.1	-11.8	672	>15	5	#Ac, 2As
13-Jun	PM6:35	sunny	NE	4.0(5.1)	-17.9	-14.3	675	>15	2	1Cu, 1-Ac, 0+St
14-Jun	AM3:45	blowing snow	NE	7.8(9.5)	-18.6	-18.2	678	0.5	Unobservable	Unobservable
14-Jun	AM5:55	blowing snow(sunny in upper air)	NE	7.9(9.9)	-17.6	-15.9	677	1~5	Unobservable	Unobservable
14-Jun	AM6:55	sunny with blowing snow	NE	5.8(7.6)	-17.0	-17.2	678	5~10	5	3St, 2Cc
14-Jun	AM7:55	sunny with blowing snow	NE	5.3(6.6)	-15.1	-16.9	677	10	2	St

filter packs were sealed in a clean plastic case, and the cases were transported manually.

For precipitation sampling, snow was collected in a polyethylene bag fitted on a 45L bucket on the snow surface from the same site as that of the aerosol sampling. Precipitation was collected during the same time period as that of the aerosol sampling. After collection, the snow was transferred to a 50 ml polypropylene bottle, and the bottles were transported in a frozen state together with the ice core. We collected 26 samples of surface snow (up to 0.02 m depth) in a polypropylene bottle, for analyses of water-stable isotopes, ion, dust concentrations, and aerosol components from the same site as that of the precipitation sampling. After sealing the bottle, the samples were transported in a frozen state together with the ice core.

On 31st May, 1st June, 2nd June, and 7th June, we conducted snow-pit observations down to a depth of 3.3 m (Fig. 3d). The observation variables were snow temperature, stratigraphy, and density. For chemical analysis, snow samples were collected at intervals of 0.05 m, and these samples were placed on a 50 ml polypropylene bottle for analyses of water-stable isotopes, ion, dust concentrations and aerosol components. On the other hand, samples were collected from up to 2.0 m below the “snow surface” at 0.20 m depth intervals in a 1000 ml polypropylene bottle for sulfate and nitrate aerosol isotopes analyses. For hard snow, we used stainless-steel tools, and each sample was placed in a separate polyethylene bag/bottle after decontamination of the surface by a ceramic knife. For major ion and stable isotope analyses, some samples were melted in Whirl pack bags and transferred to a polypropylene bottle of 50 ml in Kulusuk. The residual samples were transported in a frozen state together with the ice core.

In addition, we also concreted surface snow using 1-Bromododecane (B0587; Tokyo Chemical Industry Co., Ltd.) to fix the snow structure and avoid mechanical damage and metamorphosis during their transportation to Japan. We obtained eight samples, among which four were collected just after snowfall from the surface (i.e., 0.03 m depth), and the others were from pit wall of 0.47–0.53 m, 0.77–0.83 m, 0.97–1.03 and 1.17–1.23 m depth. We cut the snow into rectangular blocks (0.05×0.05×0.06 m) using a hand saw, and organized the blocks into a pack (Ziplock 140 ml container). Subsequently, we immersed the pack with 1-Bromododecane at -16°C , which is lower than the melting point of 1-Bromododecane (-10°C). Before being immersed, the 1-Bromododecane was kept at a temperature of -6°C using an insulating box, which is higher than its melting point. The concreted samples were transported in a frozen state, together with the ice core.

5.3 Meteorological observations

We conducted meteorological observations during our stay at the field camp using a hand-held meteorological meter (Kestrel 4500NW) (Fig. 3e). Weather, air and

surface snow temperature, air pressure, wind speed and direction, cloud type, cloud amount, and visibility were measured 116 times during the period from 9th May to 14th June (Table 2). The average and standard deviation of air pressure was 669 ± 6 hPa. The sky was clear from 9th to 21st May. However, two episodes of blizzards were encountered during 22nd May to 3rd June. During the blizzard, the northeast winds were too strong for the Kestrel to measure the wind speed (Table 2). We did not perform any drilling/sampling work during the blizzard. From 4th to 14th June, the weather condition fluctuated between sunny and snowy while it was forecasted to be sunny without snow. It is likely that the moisture forming the snow might have originated from the surface snow at the SE-Dome region, which was locally circulated without moisture transportation from other regions. The transported moisture should be considered in the numerical prediction model described in section 6.1.

We measured air temperature and humidity (HIOKI LR5001; LR9502) automatically at every 5 min from 10th May to 6th June near the camp. The sensor with a radiation shield was mounted on a pole situated at about 2 m height from the snow surface. The lowest and the highest temperatures observed were -29.3°C at 15:50 on 15th May and -2.5°C at 02:15 on 21st May, respectively; the mean temperature was -16.9°C (blue line in Fig. 4). Due to the strong blizzard on 29th May, the humidity sensor stopped recording any information (orange line in Fig. 4). Figure 4 also displays the air temperature measured by the hand-held meter (green circle in Fig. 4). The blue line and green circles displayed good correspondence for data acquired in the same date. Snow surface temperature (red circles in Fig. 4) was lower than the air temperature, especially during nighttime of sunny days. The surface was cooled to less than -30°C during some sunny days in May, probably due to radiative cooling.

5.4 Surface elevation and internal stratigraphy of SE-Dome region

A ski-oriented GPS and GPR measurements were performed to provide an estimate of the snow surface elevation and firn layer around the drilling site (Fig. 3f). Figure 5a shows our tracks covered during the course of the measurements. Overall, we walked 83 km and the mean walking speed was around 4.5 km h^{-1} . We used a dual-frequency GPS (DEM-1, GNSS technology), and fixed the antenna on our backpack. To investigate the surface topography, GPS signals were recorded at every 1 sec, which was post-processed with the PPP (Precise Point Positioning)-kinematic method to obtain three-dimensional coordinates of the antenna. We used a web application was used for recording the GPS signals provided by the Canadian Geodetic Survey (CSRS-PPP, <https://webapp.geod.nrcan.gc.ca>). The accuracy of the horizontal and vertical coordinates was ~ 0.8 m and ~ 3.5 m, respectively. Figure 5b shows the surface topography map generated

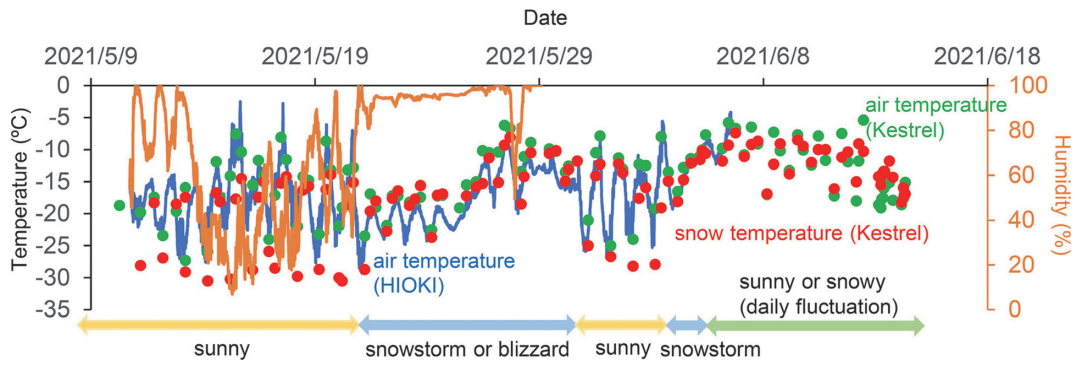


Fig. 4. Variations in the measured weather, temperature, and humidity conditions during the field study. The blue and orange lines show air temperature and humidity (HIOKI LR5001; LR9502) at every 5 min from 10th May to 6th June, respectively. The green and red circles show the air and snow temperatures measured by the hand-held meter (Kestrel), respectively.

by GPS based on our tracks. We measured the coordinate of the weather station for several days during the entire period of fieldwork to calculate the speed of ice at the surface. Using CSRS-PPP with PPP-static method, we estimated the coordinate for each observation. The ice speed was calculated to be $2.2 \pm 0.2 \text{ m a}^{-1}$.

Firn layers were measured with a GPR system (SIR4000) equipped with 100 MHz central frequency antennae (GSSI Inc., Model 3207). The system was mounted on a plastic sledge. We collected 1024 samples per trace in a 1078 ns window with a scan rate of 32 traces per second. Our average walking speed was ~ 25 traces every meter. Three-dimensional coordinates measured by the GPS were used to compute the position of each trace. The acquired GPR dataset was processed with an open-source python tool (<https://readgssi.readthedocs.io/>). Figure 5c shows an illustration of radargram along with the new and old drilling sites. Several internal reflecting horizons are visible in the figure, which can be used to calculate the spatial distribution of the accumulation rate around the SE-Dome. More detailed analysis of the radargram is planned for calculating the accumulation rate accompanied by snow/firn density profiles and chemical data obtained from the shallow ice cores.

6. Safety managements during field camp

6.1 Weather forecast for field activities

Weather forecast is integral to schedule the field activities, plan the journey, and take precautionary measures for severe weather conditions. During our field study, we received weather forecast information from two models for the SE-Dome site from the weather forecast team in Japan. The first was the 5 days weather forecast by Japan Meteorological Agency Non-Hydrostatic Model (JMA-NHM) for every 3 hours (Saito *et al.*, 2006; Hashimoto *et al.*, 2016; 2017). The second was subsequent 3 days weather forecast provided by the Japan Meteorological Agency Global Spectral Model (JMA-GSM) for every 12 hours. These weather forecasts

included weather, relative humidity, precipitation amount, wind speed and direction. We used an inReach Mini (Garmin, USA) and application Earth Mate (Garmin, USA) installed on an iPad (Apple, USA) for communicating from the field camp to Japan. Sometimes, messages detailing domestic and international news (e.g. COVID-19 status) were sent to the members of the expedition from Japan alongside the weather forecast.

6.2 Caution against polar bears

Recently, polar bears were spotted near research stations in Greenland Ice Sheet, such as in the Summit and E-GRIP stations. Therefore, there was a risk of being attacked by polar bears in our camp. According to a regulation for conducting scientific research in Greenland, we carried a rifle to fire warning shots to polar bears and shoot polar bears. Since it was difficult to know if a polar bear was approaching the camp during nighttime, we took a male dog borrowed from a hunter in Kulusuk, for alerting us in case any polar bear approached. Although we did not encounter any polar bears during our field camp, however, the dog certainly enabled us to have peaceful nights and kept us safe.

6.3 Maintenance of the field camp against severe weather condition

During the expedition, our camp was hit by strong blizzards and blowing snow several times. During the setup of the kitchen tent, we took a lot of stays in case of bad weather. However, the tent was damaged during the first blizzard. Therefore, we took additional stays and reinforced the tent. The main masts of the drill tent were not strong enough. Therefore, we reinforced the tent with timbers on 10th May. However, the strong wind on 29th May tore the bag-like parts that holds the main masts. We repaired the tent and tied the tent fabric directly to the main poles and timbers. Moreover, a couple of polycarbonate poles that form arches of the semi-cylindrical (kamaboko-) shaped tent broke and had to be replaced. Personal sleeping tents were not damaged by blizzard, however, the tents were often buried by

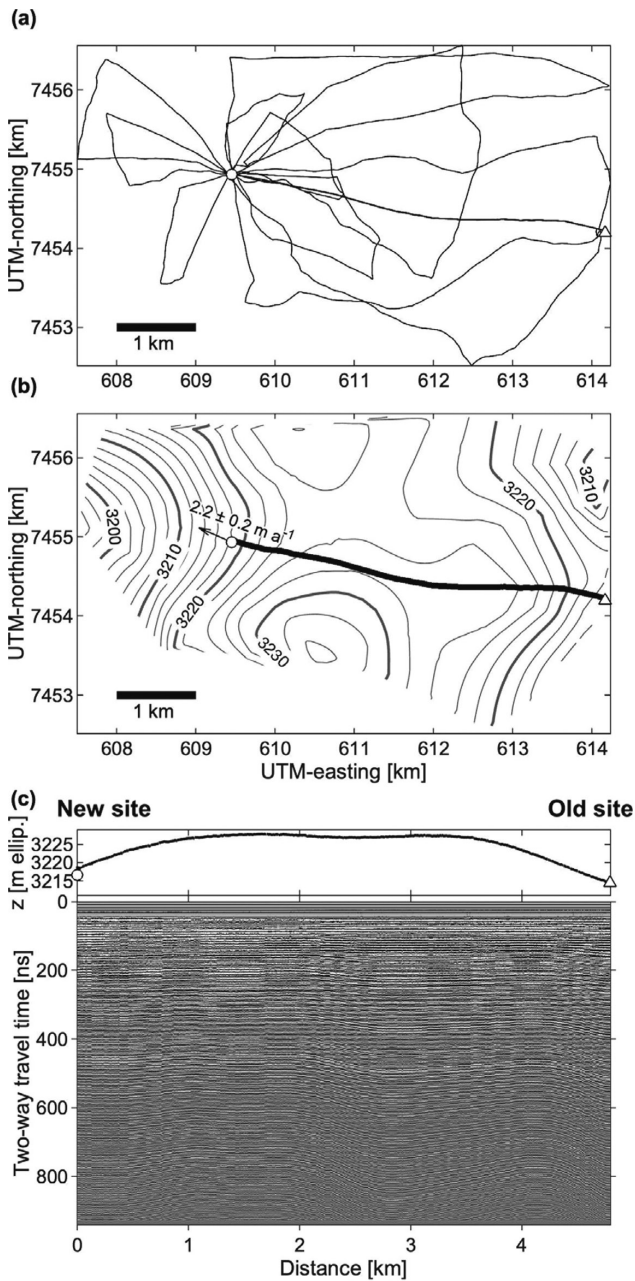


Fig. 5. (a) GPS tracks around the drilling site. Open circle and triangle indicate the new and old drilling sites, respectively. (b) Surface topography (m ellip.) with a contour level of 2 m generated from GPS measurements. Surface ice velocity at the new drilling site (open circle) is indicated by the velocity vector. Coordinates are in UTM 24 N (km). (c) An illustration of radargram obtained in this study along the line connecting the drilling sites. The black curve indicates snow surface elevation along the survey line.

snow drifts created by blizzards or blowing snow. Therefore, we had to remove the drifting snow several times and move the tents immediately after.

7. Preliminary estimation of depth-age relationship of the 250 m ice core

We estimated the depth-age relationship of the 250 m

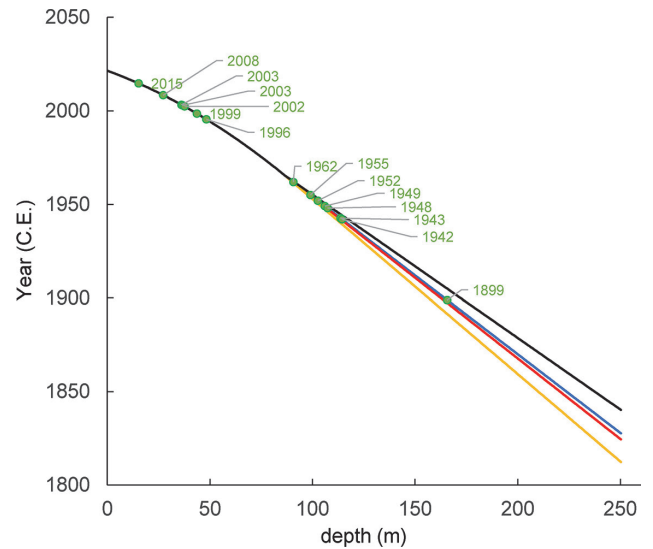


Fig. 6. Estimated depth-age relationships of ice cores. Blue curve when the ice density is 850 kg m^{-3} ; red curve when the ice density is 870 kg m^{-3} ; black curve when the ice density is 850 kg m^{-3} and accumulation rate increases by 10%; yellow curve when the ice density is 850 kg m^{-3} and accumulation rate decreases by 10%. Green circles show the depth (age) of the blue curve where ice layers were found in the ice core.

ice core. Based on stable water isotope studies on the previous ice core, we estimated the depositional ages of samples from the surface to 90 m depth in this region to be 60 years (Furukawa *et al.*, 2017). We extrapolated the relationship to the top 90 m depth of the new 250 m ice core. For estimating the ice core ages from 90 to 250 m depth, we made the following assumptions: i) the ice core sections were already closed off because the close off depth of the previous ice core was 83 m (Iizuka *et al.*, 2017); ii) the annual accumulation rate is constant at $1.01 \text{ m w.e. yr}^{-1}$, which was obtained from the previous ice core with the age of deposition being 1958 to 2014 (Furukawa *et al.*, 2017). Based on these assumptions, the depth-age relationship of samples from 90 to 250 m depth was estimated.

Figure 6 shows the estimated depth-age relationship of this ice core. When the ice core density was 850 kg m^{-3} , the age at 250 m depth was AD 1827 (blue line). In case the ice core density was 870 kg m^{-3} , the age at 250 m depth was AD 1824 (red line), and thus, there is no significant difference in age between ice cores with different densities. If annual accumulation rate increased or decreased by 10%, the ages at 250 m depth corresponded to AD 1840 (black line) and AD 1812 (yellow line), respectively. We found fifteen ice layers in the entire ice core. The ice layers, marked by green circles in Fig. 6, were mainly formed during 1940–1960 and 1995–2020. These periods are considered as warm periods in the Arctic region (IPCC 2013, AMAP 2017), and therefore, we can state that our rough dating estimation is reasonable.

Further analyses are needed to construct a more

precise timescale of the ice core. However, the rough estimation of the depth-age relationship suggests that the 250 m ice core contains paleoenvironmental proxies during Anthropocene (1850–2020). Therefore, we suggest that we have obtained enough ice core that are suitable for the purpose of the project MEXT/JSPS, KAKENHI (No. 18H05292), which aims to construct the most reliable deposited-aerosol database of the Anthropocene (i.e., from 1850 to 2020).

8. Conclusions

We drilled a 250.51 m ice core from a high accumulation region of the southeastern Greenland Ice Sheet. The 250.51 m ice core contained paleoenvironmental proxies of the Anthropocene (1850–2020), which aided in constructing a reliable deposited-aerosol database of the Anthropocene. Apart from ice core drilling, we carried out several observations, snow sampling, and measurement of surficial elevation and internal stratigraphy in the SE-Dome region. We also sampled aerosol and snow, and performed meteorological observations during the field study. The ice cores and snow samples will be transported by a 40 ft reefer, which is expected to at the Institute of Low Temperature Science of Hokkaido University by mid-october. We are now shifting from field logistics to continue scientific analyses to accomplish the remaining objective of this project, which aims to construct the most reliable deposited-aerosol database of the Anthropocene (from 1850 to 2020).

Acknowledgments

We are grateful to Kazutaka Yoshihashi (Maruzen Showa Unyu Co., Ltd.), Hiroshi Utsumi (Arctic Observation Support Organization, Inc.), George Palaima (Arctic Observation Support Organization, Inc.), and Tomoko Ryuho (Maruzen Showa Unyu Co., Ltd) for their logistical support. We appreciate the support from Bendt Duus and Kulusuk airport officials, Bendt Abelsen and Kulusuk resident relations, and Norlandair pilots for providing logistical support in Kulusuk and SE Dome. We also thank Akio Kobayashi and Yasushi Yoshise (Kyushu Olympia Kogyo Co., Ltd.) for preparing the drilling system, Manabu Fukui and administrative staffs of the Institute of Low Temperature Science, Hokkaido University for supporting the overseas business trip and Shin Sugiyama and Shuji Fujita for providing GPS and GPR used during the expedition. This study was supported by MEXT/JSPS KAKENHI Grant Number 18H05292 (and previous project number 26257201). This work was partially carried out by the Joint Research Program and the Readership program of the Institute of Low Temperature Science, Hokkaido University, and the Arctic Challenge for Sustainability (ArCS II) Project, Program Grant Number JPMXD1420318865. MM was

supported by Grant-in-Aid for JSPS Fellows (JP20J00526).

References

- AMAP (2017): Snow, Water, Ice and Permafrost in the Arctic (SWIPA) 2017. Arctic Monitoring and Assessment Programme (AMAP), Oslo, Norway. xiv + 269 pp.
- Amino, T., Iizuka, Y., Matoba, S., Shimada, R., Oshima, N., Suzuki, T., Ando, T., Aoki, T. and Fujita, K. (2021): Increasing dust emission from ice free terrain in southeastern Greenland since 2000. *Polar Sci.*, **27**, 100599, doi:10.1016/j.polar.2020.100599.
- Bamber, J. L., Griggs, J. A., Hurkmans, R. T. W. L., Dowdeswell, J. A., Gogineni, S. P., Howat, I., Mouginot, J., Paden, J., Palmer, S., Rignot, E. and Steinhage, D. (2013): A new bed elevation data-set for Greenland. *The Cryosphere*, **7**, 499–510, doi:10.5194/tc-7-499-2013.
- Burgess, E. W., Forster, R. R., Box, J. E., Mosley-Thompson, E., Bromwich, D. H., Bales, R. C. and Smith, L. C. (2010): A spatially calibrated model of annual accumulation rate on the Greenland Ice Sheet (1958–2007). *J. Geophys. Res.*, **115**, F02004, doi:10.1029/2009JF001293.
- EPICA community members. (2006): One-to-one coupling of glacial climate variability in Greenland and Antarctica. *Nature*, **444**, 195–198, doi:10.1038/nature05301.
- Fettweis, X., Hofer, S., Krebs-Kanzow, U., Amory, C., Aoki, T., Berends, C. J., Born, A., Box, J. E., Delhasse, A., Fujita, K., Gierz, P., Goelzer, H., Hanna, E., Hashimoto, A., Huybrechts, P., Kapsch, M.-L., King, M. D., Kittel, C., Lang, C., Langen, P. L., Lenaerts, J. T. M., Liston, G. E., Lohmann, G., Mernild, S. H., Mikolajewicz, U., Modali, K., Mottram, R. H., Niwano, M., Noël, B., Ryan, J. C., Smith, A., Streffing, J., Tedesco, M., van de Berg, W. J., van den Broeke, M., van de Wal, R. S. W., van Kampenhout, L., Wilton, D., Wouters, B., Ziemann, F. and Zolles, T. (2020): GrSMBMIP: intercomparison of the modelled 1980–2012 surface mass balance over the Greenland Ice Sheet. *The Cryosphere*, **14**, 3935–3958, doi: 10.5194/tc-14-3935-2020.
- Furukawa, R., Uemura, R., Fujita, K., Sjolte, J., Yoshimura, K., Matoba, S. and Iizuka, Y. (2017): Seasonal scale dating of shallow ice core from Greenland using oxygen isotope matching between data and simulation. *J. Geophys. Res.: Atmos.*, **122**, 10,873–10,887, doi:10.1002/2017JD026716.
- Hashimoto, A., Niwano, M. and Aoki, T. (2016): Numerical weather prediction supporting cryospheric field observation campaign on the Greenland Ice Sheet (in Japanese with English abstract and captions). *J. Jpn. Soc. Snow and Ice (Seppyo)*, **78**, 205–214.
- Hashimoto, A., Niwano, M., Aoki, T., Tsutaki, S., Sugiyama, S., Yamasaki, T., Iizuka, Y. and Matoba, S. (2017): Numerical weather prediction system based on JMA-NHM for field observation campaigns on the Greenland ice sheet. *Low Temperature Science*, **75**, 91–104, doi:10.14943/lowtemsci.75.91.
- Hattori, S., Iizuka, Y., Alexander, B., Ishino, S., Fujita, K., Zhai, S., Sherwen, T., Oshima, N., Uemura, R., Yamada, A., Suzuki, N., Matoba, S., Tsuruta, A., Savarino, J. and Yoshida, N. (2021): Isotopic evidence for acidity-driven enhancement of sulfate formation after SO₂ emission control. *Sci. Adv.*, **7**, eabd4610, doi:10.1126/sciadv.abd4610.
- Iizuka, Y., Matoba, S., Yamasaki, T., Oyabu, I., Kadota, M. and Aoki, T. (2016): Glaciological and meteorological observations at the SE-Dome site, southeastern Greenland Ice Sheet. *Bull. Glaciol. Res.*, **34**, 1–10, doi:10.5331/bgr.15R03.
- Iizuka, Y., Miyamoto, A., Hori, A., Matoba, S., Furukawa, R., Saito, T., Fujita, S., Hirabayashi, M., Yamaguchi, S., Fujita, K. and Takeuchi, N. (2017): A firm densification process in the high accumulation dome of southeastern Greenland. *Arctic, Antarctic, and Alpine Research*, **49**, 13–27, doi:10.1657/aar0016-034.
- Iizuka, Y., Uemura, R., Fujita, K., Hattori, S., Seki, O., Miyamoto, C., Suzuki, T., Yoshida, N., Motoyama, H. and Matoba, S. (2018): A 60 year record of atmospheric aerosol depositions preserv-

- ed in a high accumulation dome ice core, Southeast Greenland. *J. Geophys. Res.: Atmos.*, **123**, 574–589, doi:10.1002/2017JD026733.
- IPCC (2013): Climate Change 2013: The Physical Science Basis. Contribution of Working Group I to the Fifth Assessment Report of the Intergovernmental Panel on Climate Change [Stocker, T.F., D. Qin, G.-K. Plattner, M. Tignor, S.K. Allen, J. Boschung, A. Nauels, Y. Xia, V. Bex, and P.M. Midgley (eds.)]. Cambridge University Press, Cambridge, United Kingdom and New York, NY, USA, 1535 pp, doi:10.1017/CBO9781107415324.
- Kanamori, S., Benson, C. S., Truffer, M., Matoba, S., Solie, D. J. and Shiraiwa, T. (2008): Seasonality of snow accumulation at Mount Wrangell, Alaska, USA. *J. Glaciol.*, **52**, 273–278, doi:10.3189/002214308784886081.
- Saito, K., Fujita, T., Yamada, Y., Ishida, J., Kumagai, Y., Aranami, K., Ohmori, S., Nagasawa, R., Kumagai, S., Muroi, C., Kato, T., Eito, H. and Yamazaki, Y. (2006): The operational JMA Nonhydrostatic Mesoscale Model. *Mon. Weather Rev.*, **134**, 1266–1298, doi:10.1175/mwr3120.1.
- Watanabe, O., Jouzel, J., Johnsen, S., Parrenin, F., Shoji, H. and Yoshida, N. (2003): Homogeneous climate variability across East Antarctica over the past three glacial cycles. *Nature*, **422** (6931), 509–512, doi:10.1038/nature01525.
- Zatko, M., Geng, L., Alexander, B., Sofen, E. and Klein K. (2016): The impact of snow nitrate photolysis on boundary layer chemistry and the recycling and redistribution of reactive nitrogen across Antarctica and Greenland in a global chemical transport model. *Atmos. Chem. Phys.*, **16**, 2819–2842, doi:10.5194/acp-16-2819-2016.